University of Tartu
Faculty of Science and Technology
Institute of Physics

Kristi Koitla

Calculation of the surface elastic modulus tensor of tungsten using molecular dynamics method

Material science
Bachelor's thesis (12 EAP)

Supervisors: Andreas Kyritsakis, PhD
Veronika Zadin, PhD

Tartu 2024

Volframi pinna elastusustensori arvutamine molekulaardünaamika meetodiga

Nanoskaalal asuvate osakeste mehaanika uurimisel tuleb osakeste suure pindala ja ruumala suhte tõttu võtta arvesse ka pinnaefekte, mida makroskaalal ignoreeritakse. Selles töös uuritakse molekulaardünaamika meetoditega volframi pinnaenergiat, pinnapinget ja arvutatakse pinna elastsus tensorit, mis on vajalikud, et edasi uurida hulktahukalise profiili kujunemist ja nanoskoopiliste teravike tekkimist laserimpulssdega kiiritatavatel mikroskoopilisel volframtipul. Pindasid kirjeldavad suurused arvutati 4 erineva molekulaardünaamika potentsiaaliga ning neid võrreldi omavahel.
P250 Tahke aine: struktuur, termilised ja mehhaanilised omadused, kristallograafia, phase equilibria
Märksõnad *volfram, molekulaardünaamika, pinnaenergia, pinnapinge*

Calculation of the surface elastic modulus tensor of tungsten using molecular dynamics method

While studying the mechanics of nanosized objects, both the bulk and surface effects, which can be ignored on a macroscale, must be taken into account because of the high ratio of the surface to the volume of the nanoscale objects. The aim of this thesis is to calculate the surface energy, surface stress and surface elastic modulus tensor of tungsten, which is necessary to investigate the mechanism of progressive facet development and potential nanotip growth on laser-irradiated microscopic tungsten tip. The values that describe surfaces were calculated using 4 different interatomic potentials and compared.
P250 Condensed matter: structure, thermal and mechanical properties, crystallography, phase equilibria
Keywords *tungsten, molecular dynamics, surface energy, surface stress*

Contents

Acronyms and glossary of symbols

FCC — Face-Centered Cubic

BBC — Body-Centered Cubic

MD — Molecular Dynamics

CERN — European Council for Nuclear Research

CLIC — Compact LInear Collider

EAM — Embedded-Atom Method

LAMMPS — Large-scale Atomic/Molecular Massively Parallel Simulator

PBC — Periodic Boundary Conditions

1 Introduction

A recent experiment conducted by Yanagisawa et al. involved the use of femtosecond laser impulses and a strong DC electric field to irradiate a microscopic tungsten tip. This irradiation led to the gradual and reproducible development of faceted surfaces and the potential growth of nanotips. The objective of the experiment was to create nanotips using laser impulses, with the intention of utilizing these metal nanotips as sources of pulsed, bright, and coherent electron waves during laser irradiation. This approach simplifies the fabrication process compared to existing methods by allowing the laser itself to form a nanotip on a larger tip, thereby avoiding complications associated with maintaining the cleanliness of sensitive optical elements. In addition to that, understanding the mechanism of electromagnetic wave induced surface changes may help discover the process leading to vacuum breakdowns in accelerators such as the CLIC linear particle collider, which is currently in the design phase at CERN, which accelerates particles using extremely strong electric fields, where the occurrence of spontaneous vacuum breakdowns, which are theorized to be controlled by electric field-induced surface changes, limits the feasible acceleration gradient. [1]

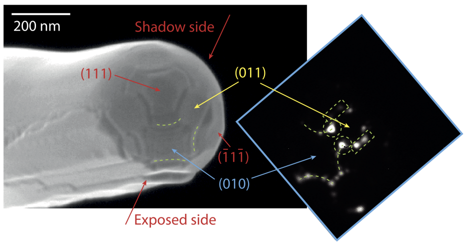

Figure 1: SEM images of the formed tungsten tip [1]

While studying the mechanics of nanosized objects, both the bulk and surface effects, which can be ignored on a macroscale, must be taken into account because of the high ratio of the surface to the volume of the nanoscale objects. To study the forming tungsten tips during irradiation a Monte Carlo simulation has been set up, but it still needs surface elastic properties of tungsten as an input to realistically model the processes that are hypothesized to be happening in the formation of the nanotip.

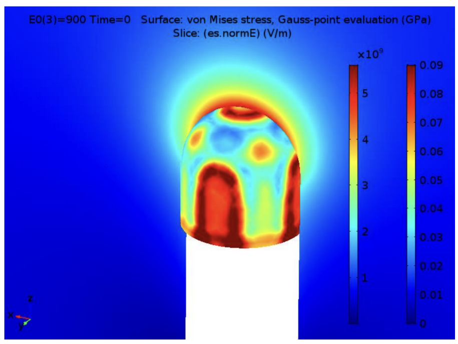

Figure 2: Current model of the nanotip [2]

Calculating the surface properties of the metal using molecular dynamics simulations before incorporating them into a Monte Carlo simulation enhances the probabilistic accuracy and computational efficiency of the Monte Carlo simulation outcomes. [2]

The aim of this thesis is to calculate the surface energy, surface stress and surface elastic modulus tensor of tungsten, which is necessary to investigate the mechanism of progressive facet development and potential nanotip growth in metals. To do that, first the surface properties of aluminium will be computed using a molecular dynamics simulation in LAMPPS software and compared with previously obtained results from literature. Then a similar simulation will be set up for tungsten and results using different interatomic potentials will be compared. In addition to that, the surface elastic constants for tungsten will be computed with additional relaxation of the metal after the straining. It is hypothesised that the surface elastic constants obtained after additional relaxing will be smaller than the ones calculated without additional relaxing time.

2 Theory

2.1 Molecular Dynamics

Molecular dynamics (MD) is a computer simulation technique that simulates the motion of each atom separately. It enables the prediction of time evolution of an interacting particular system involving the generation of atomic trajectories of a system using numerical integration of Newton's equations of motion:

$$m_i \frac{d^2 \overrightarrow{r_i}}{dt^2} = -\nabla U_i(\overrightarrow{r_1}, \overrightarrow{r_2}, ..., \overrightarrow{r_n}) \quad i \in \{1, ..., n\} \tag{1}$$

These equations relate the forces acting on an atom to its mass and acceleration. By integrating these equations over time, the positions and velocities of the atoms can be updated. Various numerical integration algorithms are used to update the atom positions and velocities at discrete time steps. The algorithms approximate the continuous trajectory of the atoms by discretizing time. [3]

2.1.1 Potential energy functions

In MD particles are treated as point masses and their pairwise interatomic interactions are described by potential energy functions, which specify the total potential energy of a system of atoms as a function of all their positions. The choice of appropriate potential energy functions is crucial to accurately representing the interatomic forces and ensuring the reliability of our simulations. [3]
For the simulations in this thesis the EAM potential functions were used. EAM potentials were chosen because they include many-body interactions that are essential for accurately capturing the nature of metallic bonding, which is particularly important at surfaces, where the coordination number of atoms changes significantly compared to the bulk material. The embedding function in EAM accounts for the local electron density, which is critical for modelling the unique electronic environment at surfaces.

2.1.2 EAM potential

The embedded-atom model/method (EAM) is a common potential function, which has been developed in order to take into consideration the coordination-dependent many-atom characteristics of metals. In this method, an atom is embedded into the local electron density that is provided by the system's remaining atoms in order to find the metal's energy. [4]
The following equation for the i-th atom's potential energy summarizes EAM interactions:

$$E_i = F_\alpha \left(\sum_{j \neq i} \rho_\beta(r_{ij}) \right) + \frac{1}{2} \sum_{j \neq i} \phi_{\alpha\beta}(r_{ij}) \tag{2}$$

where F_α is the embedding energy function that represents the energy required to place the i-th atom of type α into the electron cloud, r_{ij} is the distance between atoms i and j, $\phi_{\alpha\beta}$ is the electrostatic pair-wise function, ρ_β is the contribution to the electron charge density from atom j of type β at the location of atom i. The intricate and numerous parameters of the functional forms of F, ρ and ϕ are fitted empirically from experimental data or more accurate quantum mechanical computations. [5]
The ensemble average of a physical quantity of interest can be determined using the ergodic hypothesis from the time average over the simulation of the relevant physical quantity from the resulting trajectories, along with the velocities and forces at each timestep. This is based on the assumption that the system is in an equilibrium condition, in which case the physical quantities of interest should oscillate consistently around a mean value. [6]

2.1.3 Potential cutoff distance

Even for the simplest MD potentials, the computing cost of a simulation is typically squared as the number of atoms in the simulation is increased. For every atom in the simulation its interactions with every other atom must be considered. To minimize the number of interactions computed at each timestep a cut-off value can be used, which is a simple technique to drastically reduce calculation time. That is possible because in most systems involving short-range interactions, the potential energy and force between particles decay rapidly with distance. For example, the Lennard-Jones potential decreases with r^{-6} for attractive forces and r^{-12} for repulsive forces, where r is the distance between the particles. Most molecular dynamics potentials have a short range, influencing only a few of their closest neighbors as beyond a certain distance, interatomic interactions are effectively negligible. [7]

In addition to reducing computational costs, using a potential cutoff distance is beneficial when using periodic boundary conditions. That is to avoid having to account for multiple periodic images of the same particles in the pairwise interaction loop. [7]

2.1.4 Thermostats

In MD simulations specific thermostatic algorithms are used to keep the temperature of the system constant and add or remove energy from the boundaries of the simulation in a realistic manner. Some of the most popular are two variations of the Nosé-Hoover thermostat: canonical NVT (constant number of particles, volume, and temperature) and isothermal-isobaric NPT (constant number of particles, pressure, and temperature) ensembles.[8]

In the NVT ensemble, the total number of atoms or molecules in the simulation box remains fixed, the size of the simulation box is fixed, which means that the system's volume does not change during the simulation and the system is kept at a constant temperature. This type of thermostat is commonly used in simulations to study equilibrium and thermodynamic properties. [9]

In the NPT ensemble, the system's pressure and temperature are kept constant, allowing the volume of the simulation box to adjust as needed. This type of ensemble is used to simulate systems in which pressure and temperature are controlled variables, as in many laboratory experiments and industrial processes. [3]

The main idea of the Nosé-Hoover thermostat is adding a fictive particle, which acts as an external system, to a Hamiltonian consisting of N atoms. The temperature of the system can be controlled by heat exchange between the physical and external systems. The connection between these two systems is controlled by the effective mass, which also impacts the oscillation of the system temperature. This type of thermostat guarantees a Maxwell-Boltzmann velocity distribution for the simulation. [10 – 11]

2.2 Surface mechanics

While studying the mechanics of nanosized objects, both the bulk and surface effects, which can be ignored on a macroscale, must be taken into account due to the high ratio of the surface to the volume of the nanoscale objects. A larger fraction of the atoms or molecules in a nanoscale object are located at or close to the surface because of the high surface-to-volume ratio. The total mechanical characteristics of the material can be considerably impacted by the behavior of the surface atoms or molecules as a result of this. [12]

For instance, the mechanical response of nanomaterials is significantly influenced by surface stress, surface energy, and surface diffusion. Deformations, changes in the stability of nanoscale structures, and even surface-driven phase transitions can all be brought on by surface stress. Nanoparticles or nanofilms' adhesion, cohesion, and surface reactivity are all impacted by surface energy. [12]

Although useful for investigating materials, surface stress and surface elastic constants are difficult to determine experimentally. There have been multiple experimental methods developed to measure surface stress but all of them come with their difficulties. For example the experimental procedure of creating suitable samples to analyse by evaporating gold onto a carbon substrate may contaminate the surface, leading to an adsorbate-induced change in surface stress. When using thin films or small nanoparticles the surface stress values measured are not reliable due to the change of lattice parameters compared to bulk. [13] For example, for platinum particles with an average diameter of 10 nm, a lattice contraction of about 0.5% was measured, which significantly reduces the surface stress [14].

2.2.1 Surface energy

The additional energy per unit area of a material's surface relative to the energy of the bulk is known as surface energy, surface free energy or surface tension. It stands for the energy difference between the atoms or molecules on the material's surface and those in the interior of the material. In a solid substance, atoms and molecules naturally want to arrange themselves in a way that reduces the system's

overall energy. Atoms are surrounded by other atoms in a bulk material, which results in a balanced distribution of attraction and repulsive forces. However, at the surface, atoms are isolated from neighbors on one side, leading to imbalanced forces and increased energy. Surface relaxation is the process by which the atoms of the newly formed crystal surfaces caused by a split or cleavage shift rearrange at the nanoscale. Since a more stable surface results from relaxing, the energy of the relaxed surface is always lower than that of the unrelaxed surface. [15 – 16]
Surface energy of a material can be calculated using the following formula

$$\gamma = \frac{E_{tot} - E_b}{2A} \tag{3}$$

where E_{tot} is the total energy of the system with surface, E_b is the total energy of the bulk system without surface, and A is the surface area. The number of atoms in both systems should be the same. [17]
The total energy of the surface can then be evaluated with the following formula:

$$E_s = A\gamma(\epsilon) \tag{4}$$

The total surface energy as a function of strain and numerical differentiation of the necessary quantities are used to construct the surface stress tensor and elastic tensor. Strain here is defined as follows:

$$\epsilon = \frac{1}{2}(F^T F - I) \tag{5}$$

where F is the deformation gradient and I is the identity matrix. [18]
The strain energy in the bulk and the surface energy make up the system's total energy when a block of material is strained. It is necessary to separate the surface energy from the overall energy. The total energy of the system can be expressed as:

$$E_{tot} = 2A\gamma(\epsilon) + hAW(\epsilon) \tag{6}$$

where A is the surface area of the free surfaces at the top and bottom of the block of material, $\gamma(\epsilon)$ is the surface energy, $W(\epsilon)$ is the bulk strain energy density and h is the thickness. In this formula $2A\gamma(\epsilon)$ represents the energies of the 2 surfaces and $hAW(\epsilon)$ is the energy in the bulk material. In the simulations the thickness of the block of material should be determined by a Gibbs dividing surface construction so that the total energy of the system would depend linearly on the thickness. To calculate the surface elastic properties, a simulation cell as shown in figure 4 would be constructed. [19]

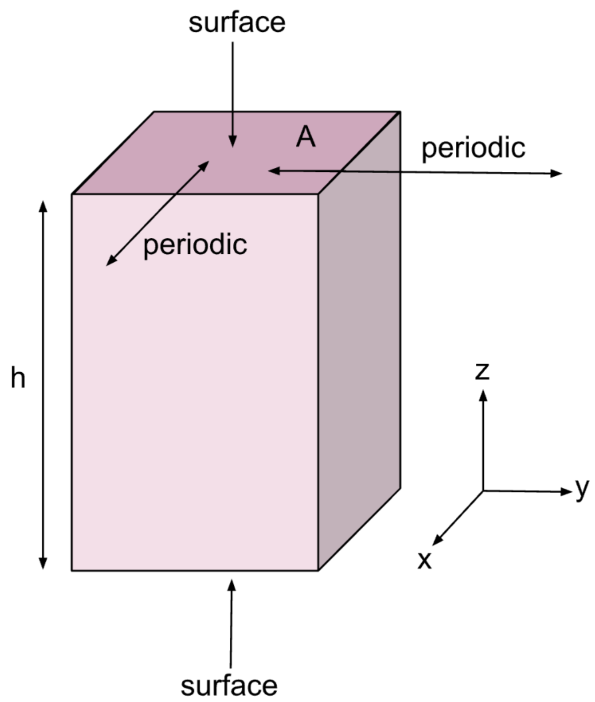

Figure 3: Schematic of a simulation cell used to determine surface elastic properties of a block of material of thickness h and area A. Periodic boundary conditions are used in the x and y directions.

2.2.2 Surface stress

Surface stress (τ) measures the forces that exist at the surface of a material with respect to strain. Surface stress, unlike thin-film stress, does not depend on thickness since the surface effect is calculated per surface area rather than volume. As a result, surface stress can be considered an intrinsic characteristic of the surface. The relationship between surface stress and surface energy (γ) is demonstrated by the following equation:

$$\tau(\epsilon) = \gamma + \frac{\partial \gamma}{\partial \epsilon} \tag{7}$$

Surface stress is the variation in total surface energy per unit area with respect to the strain and can also be written as follows:

$$\tau = \frac{1}{A}\frac{\partial E_s}{\partial \epsilon} \tag{8}$$

where the area A stands for initial area before deformations. [20]
From equation 8 surface stress at 0 strain can be written as

$$\tau_0 = \left(\frac{1}{A}\frac{\partial E_s}{\partial \epsilon}\right)_{\epsilon=0} \tag{9}$$

Surface stress can also be evaluated using surface elastic constant as follows:

$$\tau = \tau_0 + S\epsilon \tag{10}$$

where S denotes the surface elastic constant of the material. [19]

2.2.3 Surface elastic constants

The change in surface stress with strain is determined by the surface elastic constants. Surface elastic constants are parameters that describe the mechanical response of a material's surface to applied stresses and the resulting strains. They provide information about the material's elasticity at the surface and are used to characterize the behavior of surfaces. From equation 10 surface elastic constants can be derived as:

$$S = \left.\frac{\partial \tau}{\partial \epsilon}\right|_{\epsilon=0} \tag{11}$$

Surface elastic constants can also be defined as second-order derivatives of surface energy with respect to the strain as follows:

$$S = \left.\frac{1}{A}\frac{\partial^2 E_s}{\partial \epsilon^2}\right|_{\epsilon=0} - \tau_0 \tag{12}$$

[19]

2.3 Crystal structure

Metals and many other kinds of materials have crystalline structures, which means that their atoms are organized in a pattern that repeats indefinitely. The placement of the atoms in a crystal is called its crystal structure. The smallest repeating unit with complete crystal structural symmetry is known as a unit cell. The crystal structure is created by packing atoms into the unit cell and then iterating the resultant pattern endlessly in all directions. The unit cell's dimensions a, b, c and internal angles α, β, γ describe it, creating a parallelepiped geometry for the unit cell. [21]

Crystallographic orientations and planes are generally described by Miller indices according to the substance's unit cell edges (Face-Centered Cubic (FCC) for aluminium and Body-Centered Cubic (BCC) for tungsten). The Miller indices of a plane are defined using the three lattice vectors. For cubic crystal systems, the lattice vectors are chosen along the edges of the crystallographic unit cell. Any crystal plane intercepts the axes at particular spots. The Miller indices are the ratios of these points, represented by a triplet of integer values (hkl). A Miller index of 0 indicates that the plane is parallel to the respective axis and negative indices are denoted by a bar over the number. When written using square brackets, Miller indices denote a crystallographic direction rather than a plane. [22]

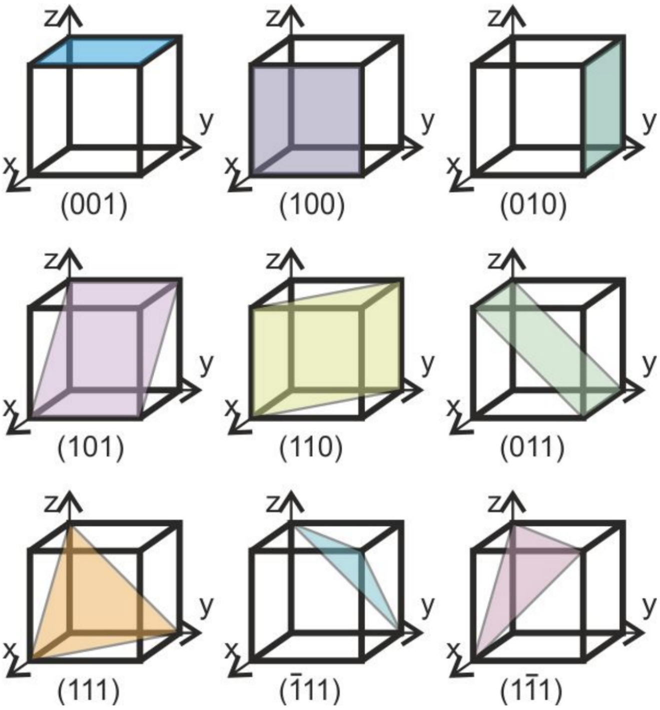

Figure 4: Examples of Miller indices indicating the plane perpendicular to the vector given for the cubic structure. [23]

The surface of a metal experiences stress due to the missing bonds on the side exposed to the vacuum, therefore crystallographic directions play a significant role in the surface properties of the material in question. Crystal surfaces with low Miller indices have in general a lower surface energy than those with high Miller indices, which is why a crystals are often surrounded by low index surfaces. [17]

3 Methodologies

3.1 The simulation setup

MD computer simulations were performed using LAMMPS open-source software [24] and visualisation of the results were done by OVITO [25].
The potential files used were obtained from the OpenKIM repository of interatomic potentials [26]. Calculations for aluminium were carried out with a potential that was developed by Ercolessi and Adams in 1994 [27]. For tungsten 4 different EAM potentials were used for comparison of the results. The potentials used were developed by Olsson in 2009 [28], Mason, Nguyen-Manh and Becquart in 2017 [29], Marinica, Ventelon and Gilbert in 2017 [30] and by Zhou, Johnson and Wadley in 2004 [31].
For the calculations, a simulation box was initially set up by specifying the lattice type as FCC and the lattice constant as 4.0479 Å for aluminium and later on as BBC and the lattice constant as 3.165 Å for tungsten [22 – 32]. The crystallographic faces that were being studied were oriented so that their surface was tangent to the z-direction. Atoms were positioned at the lattice points and their coordinates were recorded once the box dimensions were determined in unit cells. All the simulations were performed with a time step of 1 fs.
Before performing the calculations, the simulation system was relaxed until the total energy of the system stopped fluctuating and remained nearly constant. The simulation box was allowed to achieve a thermal equilibrium by thermal expansion using an integration approach based on the NPT ensemble in order to simulate a real-world system. Eventually, the atoms received a distribution of velocities that enabled them to statistically mimic temperature; at this time, the simulation box was able to expand in any direction. The simulations were conducted at a temperature of 0.1 K for aluminium and at 10 K for tungsten. It was not possible to run the simulations for tungsten at 0.1 K because the chosen potentials were not able to produce physically correct results at such low temperature. So a slightly higher, experimentally more achievable temperature was chosen. But the temperaure for aluminium was left at 0.1 K to facilitate the reproduction of previously published results.

Periodic Boundary Conditions (PBC) were established, which generated virtual duplicates of the original simulation box on each side of it. This was necessary for the system to accurately depict the properties of bulk materials at a lower computational cost. To simulate surface and bulk materials 2 separate simulations were set up: one with PBC in all directions to simulate bulk material and one which initially had PBC in all 3 directions but after the first relaxing period the box was scaled in z direction to create surfaces on both sides of the slab as shown in figure 4. After the creation of surfaces the system was allowed to relax with NVT ensamble for additional timesteps.
Figure 5 shows a simulation cell used to calculate surface energy and surface stress at 0 strain with the surfaces (110) being created in z direction and PBC remaining in the x an y directions.

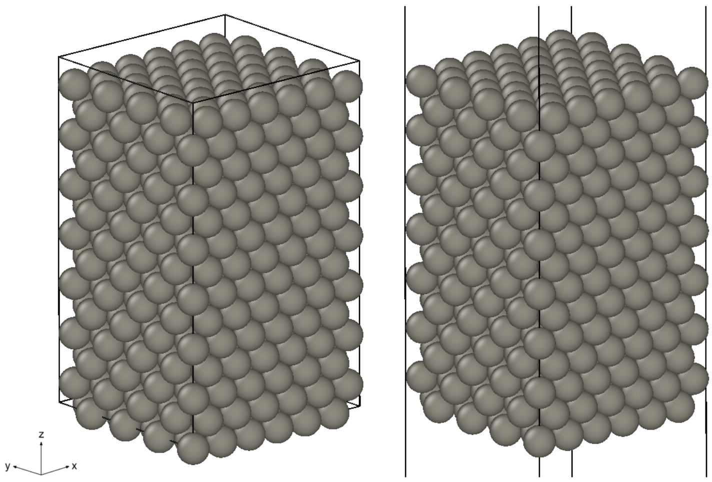

Figure 5: Simulation cell before and after the creation of surfaces.

3.1.1 Calculating surface energy

After the simulation was set up according to the parameters previously mentioned, the surface energy was calculated from the energy differences of the bulk and surface systems using formula 3.

3.1.2 Calculating surface stress tensor at 0 strain

After the simulation was set up according to the parameters previously mentioned, τ^0 values were obtained by converting the LAMMPS output pressures in the wanted directions to forces and normalizing them for used simulation box lenght.

3.1.3 Calculating surface elastic modulus tensor

After the theoretically calculated surface energy was confirmed by experimental values, the system was scaled in the x-direction with an appropriate strain value. The box length in the x-direction and energy values of the system were recorded on each timestep and used to calculate the metal's surface elastic tensor.
The x-directional length and energy values were plotted for both surface and bulk systems and fitted with second degree parabolas. The following parabolas were then retrieved:

$$E_b = a_b x^2 + b_b x + c_b$$

$$E_{tot} = a_{tot} x^2 + b_{tot} x + c_{tot}$$

where E_b represents a parabola describing the total energy of the bulk system depending on the box length in the x-direction and E_{tot} describes the same for a system with surfaces. To obtain a function describing the energy of a corresponding surface, the 2 parabolas must be substracted and divided by 2.

$$E_s = \frac{E_{tot} - E_b}{2} = \frac{a_{tot} - a_b}{2} x^2 + \frac{b_{tot} - b_b}{2} x + \frac{c_{tot} - c_b}{2}$$

To simplify the obtained expression we can make the following substitutions:

$$\frac{a_{tot} - a_b}{2} = a, \quad \frac{b_{tot} - b_b}{2} = b, \quad \text{and} \quad \frac{c_{tot} - c_b}{2} = c$$

To express surface energy in terms of the surface energy function we must use the value of surface energy function at x_0, where the surface has not been strained yet.

The initial area of the surface can be substituted as $A = x_0 y_0$.

$$\gamma = \frac{E_s(x_0)}{x_0 y_0} = \frac{a x_0^2 + b x_0 + c}{x_0 y_0}$$

To express the surface energy at 0 strain based on equation 9 we must convert the derivative with respect to ϵ to a derivative with respect to variable x which is used in the surface energy function E_s.

$$\left.\frac{\partial E_s}{\partial \varepsilon}\right|_{\varepsilon=\varepsilon_0} = \left.\frac{\partial E_s}{\partial x}\frac{\partial x}{\partial \epsilon}\right|_{\varepsilon=\varepsilon_0} = \left.\frac{\partial E_s}{\partial x}\right|_{x=x_0} \left.\frac{\partial x}{\partial \epsilon}\right|_{\varepsilon=\varepsilon_0} = \left.\frac{\partial E_s}{\partial x}\right|_{x=x_0} x_0$$

Plugging it in to the original formula 9, we get the following expression for τ_0:

$$\tau_0 = \left.\frac{\partial E_s}{\partial \varepsilon}\right|_{\varepsilon=\varepsilon_0} \cdot \frac{1}{x_0 y_0} = \left.\frac{\partial E_s}{\partial x}\right|_{x=x_0} x_0 \cdot \frac{1}{x_0 y_0} = \frac{2 a x_0 + b}{y_0}$$

And finally to get the formula for the components of the surface elastic modulus tensor from equation 12 we must convert the second derivative with respect to ϵ to a derivative with respect to variable x.

$$\left.\frac{\partial^2 E_s}{\partial \varepsilon^2}\right|_{\varepsilon=0} = \left.\frac{\partial^2 E_s}{\partial x^2}\left(\frac{\partial x}{\partial \epsilon}\right)^2\right|_{\varepsilon=0} + \left.\frac{\partial E_s}{\partial x}\frac{\partial^2 x}{\partial \epsilon^2}\right|_{\varepsilon=0} = \left.\frac{\partial^2 E_s}{\partial x^2}\right|_{x=x_0} x_0^2 - x_0 \cdot \left.\frac{\partial E_s}{\partial x}\right|_{x=x_0}$$

By substituting the obtained result into equation 12 and simplifying we get the following expression for calculating the components of surface elastic modulus tensor:

$$S = \frac{1}{x_0 y_0}\left.\frac{\partial^2 E_s}{\partial \varepsilon^2}\right|_{\varepsilon=0} - \tau_0 = \frac{1}{x_0 y_0}\left[\frac{\partial^2 E_s}{\partial x^2} \cdot x_0^2 - x_0 \cdot \frac{\partial E_s}{\partial x}\right] - \tau_0 = \frac{2 a x_0}{y_0} - 2\tau_0$$

Similar method was used to obtain the values for stretching in the y direction. For the relaxed case, after stretching the box additional relaxing with NVT ensamble was applied and then the surface elastic constants were calculated using equation 10.

3.2 Choosing the dimensions of the simulation box

From equation 6 we can see that the thickness of the slab and the total energy of the system follow a linear relationship. It is important that the thickness of the slab for the simulations is chosen to be large enough so that the surfaces on each side would not influence each other. The graph in figure 6 was used to verify that the simulation system follows the linear connection from equation 3.
The E_{tot} vs. h data is fitted with a linear curve, the intercept of which is equal to twice the value of surface energy. It is visible that the data follows a close linear relationship.

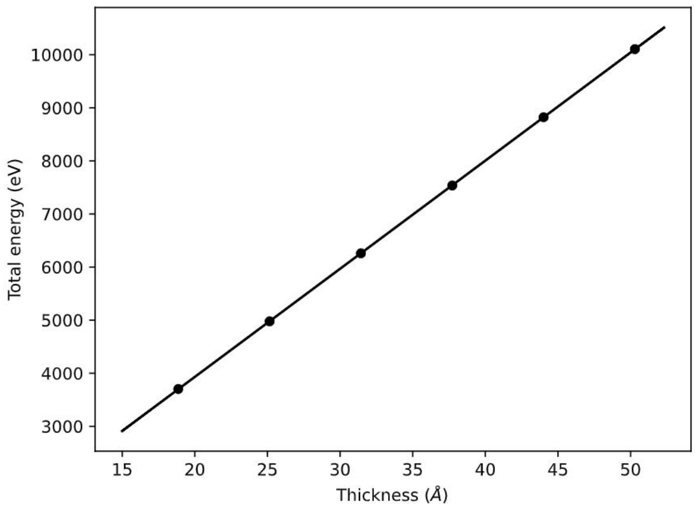

Figure 6: Total energy dependence on thickness on a 18.86 Å x 18.86 Å block of material with surface crystal orientation of (100).

4 Results and discussion

4.1 Surface energies and surface stress tensors

In this section the results of the calculations using EAM potentials to determine the surface stress tensor and the surface elastic constants are presented. The following four surface orientations were studied: (001), (111), (110) and (112). The first rows of the following tables show the values that were calculated for aluminium to validate the values obtained from the simulation methodology that was used. All of the values of surface energy calculated for aluminium matched exactly with the values reported by Shenoy and the calculated values of surface stress at 0 strain had a 0.1% or smaller difference compared to the values reported by Shenoy. The following rows show values calculated for tungsten using 4 different potentials. Calculations made with the potential developed by Olsson is marked in the results tables with W(O), potential developed by Mason, Nguyen-Manh and Becquart is marked with W(MNB), potential developed by Marinica, Ventelon and Gilbert is marked by W(MVG) and the potential developed by Zhou, Johnson and Wadley is marked by W(Z).

Table 1: Surface stress tensor of the (001) crystal face. The "1" direction corresponds to [100] and "2" corresponds to [010].

Element	$\gamma \left(\frac{eV}{\mathring{A}^2}\right)$	$\tau_{11}^0 \left(\frac{eV}{\mathring{A}^2}\right)$	$\tau_{22}^0 \left(\frac{eV}{\mathring{A}^2}\right)$	$\tau_{12}^0 \left(\frac{eV}{\mathring{A}^2}\right)$
Al	0.0588	0.03556	0.03555	0
W(O)	0.212028	0.126451	0.137232	0
W(MNB)	0.264327	0.227565	0.214551	0
W(MVG)	0.207359	0.1242	0.123965	0
W(Z)	0.217406	0.190536	0.180623	0

In table 1 the surface energy computed using the potential developed by Mason, Nguyen-Manh and Becquart is significantly higher than the others. The differences in τ_{11}^0 and τ_{22}^0 values calculated with every potential are minimal.

Table 2: Surface stress tensor of the (111) crystal face. The "1" direction corresponds to $[1\bar{1}0]$ and "2" corresponds to $[11\bar{2}]$.

Element	$\gamma \left(\frac{eV}{\mathring{A}^2}\right)$	$\tau_{11}^0 \left(\frac{eV}{\mathring{A}^2}\right)$	$\tau_{22}^0 \left(\frac{eV}{\mathring{A}^2}\right)$	$\tau_{12}^0 \left(\frac{eV}{\mathring{A}^2}\right)$
Al	0.0543	0.05685	0.05685	0
W(O)	0.204918	-0.01292	-0.007702	0
W(MNB)	0.25781	0.229628	0.230223	0
W(MVG)	0.200751	0.079281	0.071543	0
W(Z)	0.203978	-0.005367	-0.006307	0

In table 2 two of the potentials used produced negative values for the surface stress at 0 strain. Positive values of surface stress indicate tension, while negative values indicate additional compression of the material caused by the creation of surfaces.

Table 3: Surface stress tensor of the (110) crystal face. The "1" direction corresponds to [001] and "2" corresponds to $[1\bar{1}0]$.

Element	$\gamma \left(\frac{eV}{\mathring{A}^2}\right)$	$\tau_{11}^0 \left(\frac{eV}{\mathring{A}^2}\right)$	$\tau_{22}^0 \left(\frac{eV}{\mathring{A}^2}\right)$	$\tau_{12}^0 \left(\frac{eV}{\mathring{A}^2}\right)$
Al	0.0647	0.07311	0.10056	0
W(O)	0.220286	0.073105	-0.020465	0
W(MNB)	0.280757	0.27985	0.270323	0
W(MVG)	0.156641	0.119868	0.00633	0
W(Z)	0.217726	0.123738	0.000519	0

The values of τ_{11}^0 and τ_{22}^0 are much greater for W(MNB) compared to the values calculated with other potentials. In the results for other potentials all of the τ_{22}^0 values are noticably smaller than τ_{11}^0 values.

Table 4: Surface stress tensor of the (112) crystal face. The "1" direction corresponds to $[1\bar{1}0]$ and "2" corresponds to $[11\bar{1}]$.

Element	$\gamma \left(\frac{eV}{\mathring{A}^2}\right)$	$\tau_{11}^0 \left(\frac{eV}{\mathring{A}^2}\right)$	$\tau_{22}^0 \left(\frac{eV}{\mathring{A}^2}\right)$	$\tau_{12}^0 \left(\frac{eV}{\mathring{A}^2}\right)$
Al	0.0633	0.05439	0.06805	0
W(O)	0.202209	0.049765	0.008164	0
W(MNB)	0.257605	0.26666	0.261316	0
W(MVG)	0.186588	0.086319	0.059205	0
W(Z)	0.204047	0.070424	0.022059	0

In table 4 the τ_{11}^0 and τ_{22}^0 values calculated with MNB potential have much larger values than the ones that were obtained using other potentials.
It is visible from the obtained values for surface energy and surface stress can vary quite a lot based on the potentials used to set up the simulation and can even have different signs. The same observation was made in previous studies comparing different potentials as well. [19 – 33]
The potential developed by Marinica, Ventelon and Gilbert has the highest values for surface energy for every orientation studied and the obtained surface stresses have the least variation between different orientations compared to other potentials.
The surface energy values obtained in this study stay in the same range as previously reported values using different methodologies. For example in a study that used density functional theory to calculate the surface energies for tungsten the calculated values for different crystal directions stayed between 0.2277 $\frac{eV}{\mathring{A}^2}$ and 0.2748 $\frac{eV}{\mathring{A}^2}$ [34].

4.2 Surface elastic tensors

Surface elastic constants are affected by the potentials, temperatures and other variables used to set up the simulation even more than surface energies and surface stresses at 0 strains. The method of calculating surface elastic constants proposed by Shenoy, which was followed in this thesis, is computationally efficient but does not provide the most accurate numerical values. Due to the volatile nature of the surface elastic constants and little information provided in the article by Shenoy on the simulation setup and exact data used to calculate surface elastic tensors, the obtained values for aluminium only matched the values provided in the article by order of magnitude.
The difference of surface elastic constants calculated by molecular dynamic simulations using different potentials is also brought out in the study by Pishkenari and Nejat. [35]
The following tables and graphs show the exact values of the surface elastic modulus tensors obtained for all the potentials without additional relaxing after the stretching, marked in the table as UR and with additional relaxing after stretching

marked with R.

Table 5: Surface elastic modulus tensor of the (001) crystal face. The "1" direction corresponds to [100] and "2" corresponds to [010].

	$S_{1111}\left(\frac{eV}{\mathring{A}^2}\right)$		$S_{2222}\left(\frac{eV}{\mathring{A}^2}\right)$		$S_{1122}\left(\frac{eV}{\mathring{A}^2}\right)$		$S_{2211}\left(\frac{eV}{\mathring{A}^2}\right)$	
Element	UR	R	UR	R	UR	R	UR	R
Al	-0.768	-0.051	-0.769	-0.050	-0.211	-0.050	-0.203	-0.050
W(O)	-2.167	-0.028	-1.680	-0.025	-1.659	-0.014	-2.188	-0.039
W(MNB)	-4.342	-0.118	-3.991	-0.094	-4.017	-0.107	-4.316	-0.105
W(MVG)	-2.255	-0.061	-2.128	-0.066	-2.129	-0.066	-2.254	-0.060
W(Z)	-1.222	-0.028	-2.362	-0.076	-2.383	-0.087	-1.202	-0.018

All of the values in table 5 are negative. The values calculated with MNB potential have a much larger absolute value than the ones calculated with other potentials.

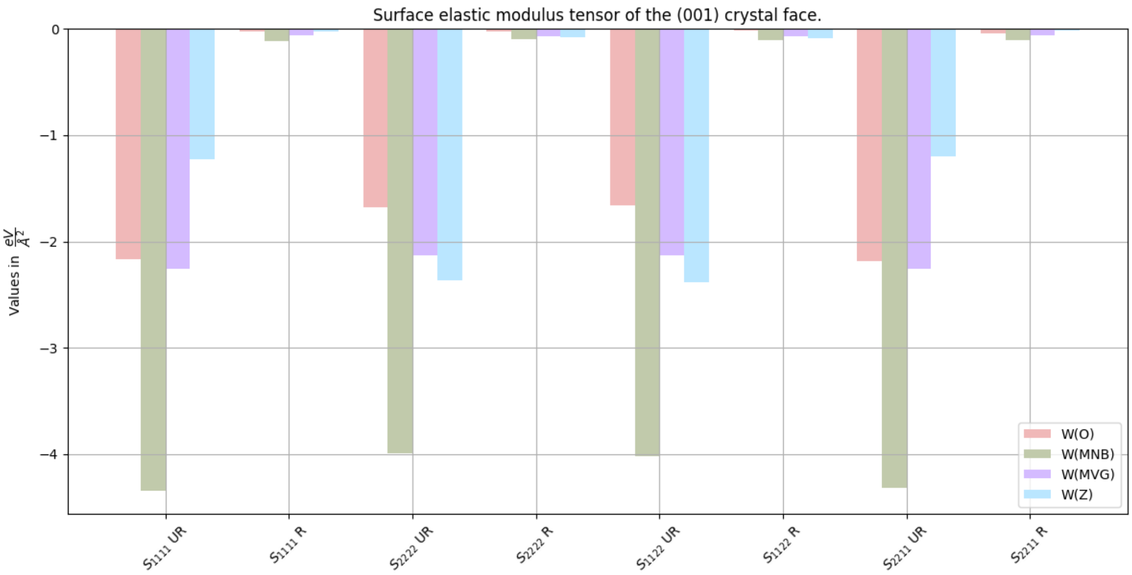

Figure 7: Graphic representation of the surface elastic modulus tensor of the (001) crystal face.

From the graphic representation of the values of the surface elastic modulus tensor in figure 7 is it clear that the relaxed and unrelaxed values follow similar trends, with the relaxed values being significantly smaller in absolute value.

Table 6: Surface elastic modulus tensor of the (111) crystal face. The "1" direction corresponds to $[1\bar{1}0]$ and "2" corresponds to $[11\bar{2}]$.

	$S_{1111}\left(\frac{eV}{\mathring{A}^2}\right)$		$S_{2222}\left(\frac{eV}{\mathring{A}^2}\right)$		$S_{1122}\left(\frac{eV}{\mathring{A}^2}\right)$		$S_{2211}\left(\frac{eV}{\mathring{A}^2}\right)$	
Element	UR	R	UR	R	UR	R	UR	R
Al	-0.117	-0.021	0.212	-0.159	0.212	-0.158	0.212	-0.158
W(O)	-1.371	-0.120	-2.152	-0.007	-2.340	-0.101	-1.184	-0.026
W(MNB)	-1.938	-0.097	-1.855	-0.225	-1.853	-0.224	-1.939	-0.097
W(MVG)	0.279	-0.045	-1.083	-0.041	-1.099	-0.049	0.294	-0.036
W(Z)	-1.798	-0.003	-2.658	-0.021	-2.660	-0.021	-1.795	-0.003

For direction (111) the table has two positive values for tungsten, both in unrelaxed state calculated with the MVG potential. Which suggest that the choice of potential can significantly influence the predicted elastic properties of the (111) crystal face.

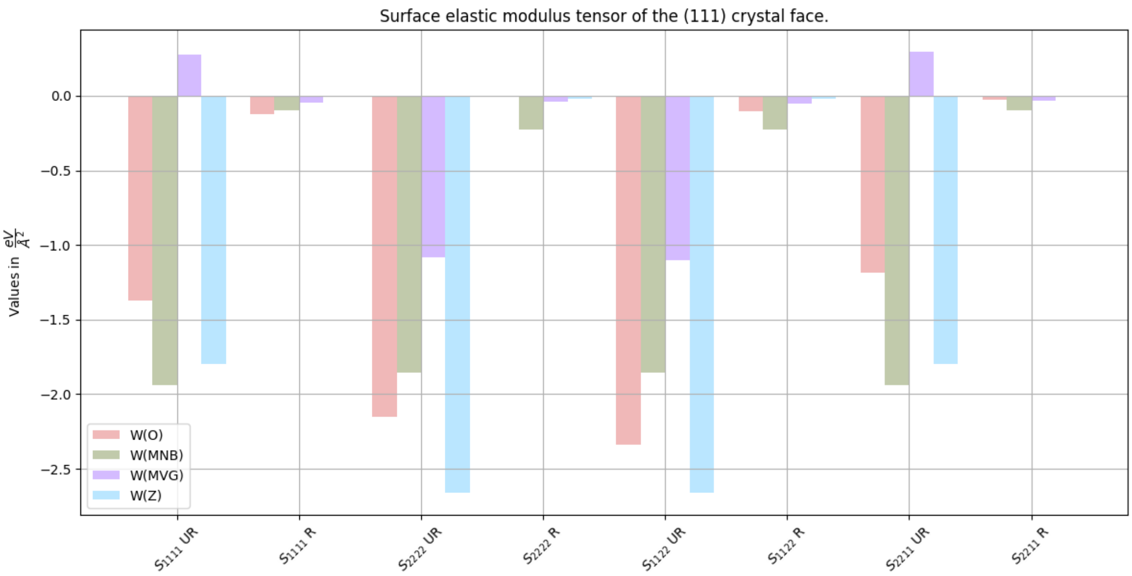

Figure 8: Graphic representation of the surface elastic modulus tensor of the (111) crystal face.

Table 7: Surface elastic modulus tensor of the (110) crystal face. The "1" direction corresponds to [001] and "2" corresponds to $[1\bar{1}0]$.

	$S_{1111}\left(\frac{eV}{\mathring{A}^2}\right)$		$S_{2222}\left(\frac{eV}{\mathring{A}^2}\right)$		$S_{1122}\left(\frac{eV}{\mathring{A}^2}\right)$		$S_{2211}\left(\frac{eV}{\mathring{A}^2}\right)$	
Element	UR	R	UR	R	UR	R	UR	R
Al	-0.167	-0.005	-1.045	-0.991	-0.222	-0.032	-0.229	-0.027
W(O)	-2.616	-0.002	-2.451	-0.038	-2.639	-0.131	-2.428	0.091
W(MNB)	-5.759	-0.140	-2.874	-0.103	-2.894	-0.112	-5.740	-0.130
W(MVG)	-3.162	-0.076	0.147	-0.014	-0.079	-0.127	-2.935	0.036
W(Z)	-2.034	-0.021	-1.703	-0.062	-1.950	-0.185	-1.788	0.101

For direction (110) the values calculated with MNB potential have a significany larger absolute value than the ones calculated using other potentials. For the S_{2211} direction in the relaxed case the calculated values were predominantly positive.

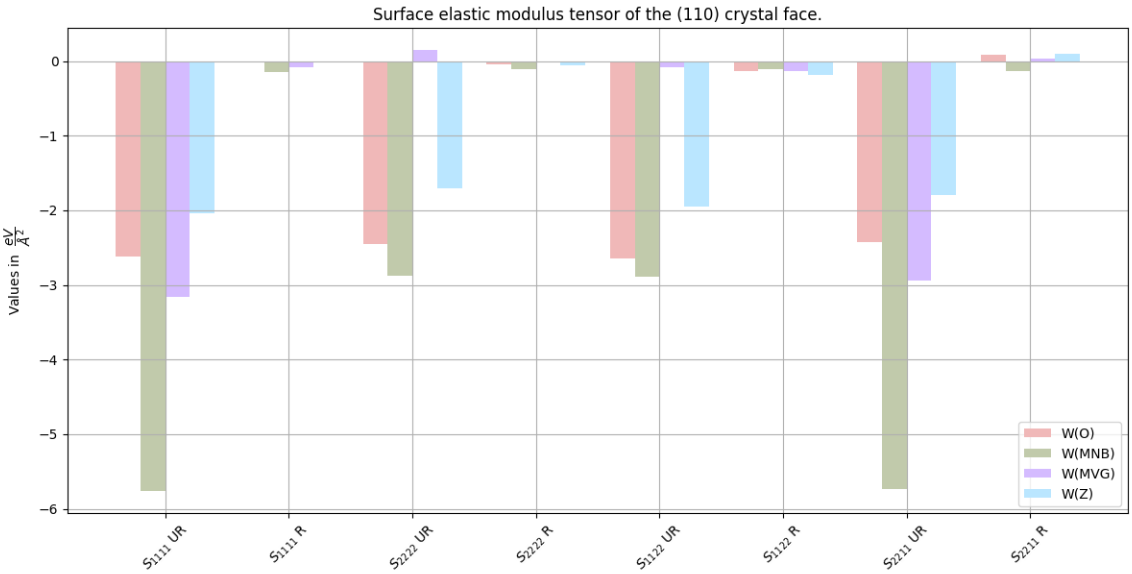

Figure 9: Graphic representation of the surface elastic modulus tensor of the (110) crystal face.

Table 8: Surface elastic modulus tensor of the (112) crystal face. The "1" direction corresponds to $[1\bar{1}0]$ and "2" corresponds to $[11\bar{1}]$.

	$S_{1111}\left(\frac{eV}{\mathring{A}^2}\right)$		$S_{2222}\left(\frac{eV}{\mathring{A}^2}\right)$		$S_{1122}\left(\frac{eV}{\mathring{A}^2}\right)$		$S_{2211}\left(\frac{eV}{\mathring{A}^2}\right)$	
Element	UR	R	UR	R	UR	R	UR	R
Al	-0.162	-0.141	-0.433	-0.121	-0.432	-0.189	-0.432	-0.118
W(O)	-2.352	-0.0768	-1.286	-0.0202	-1.369	-0.0618	-2.269	-0.035
W(MNB)	-2.663	-0.093	-2.847	-0.701	-2.858	-0.712	-2.653	-0.088
W(MVG)	-0.784	-0.047	-0.694	-0.039	-0.749	-0.065	-0.730	-0.020
W(Z)	-2.069	-0.088	-1.445	-0.028	-1.541	-0.077	-1.972	-0.040

All of the obtained surface elastic tensor components for direction (112) are negative. The values computed with MNG potential without additional relaxing have much larger absolute values than the values calculated using other potentials.

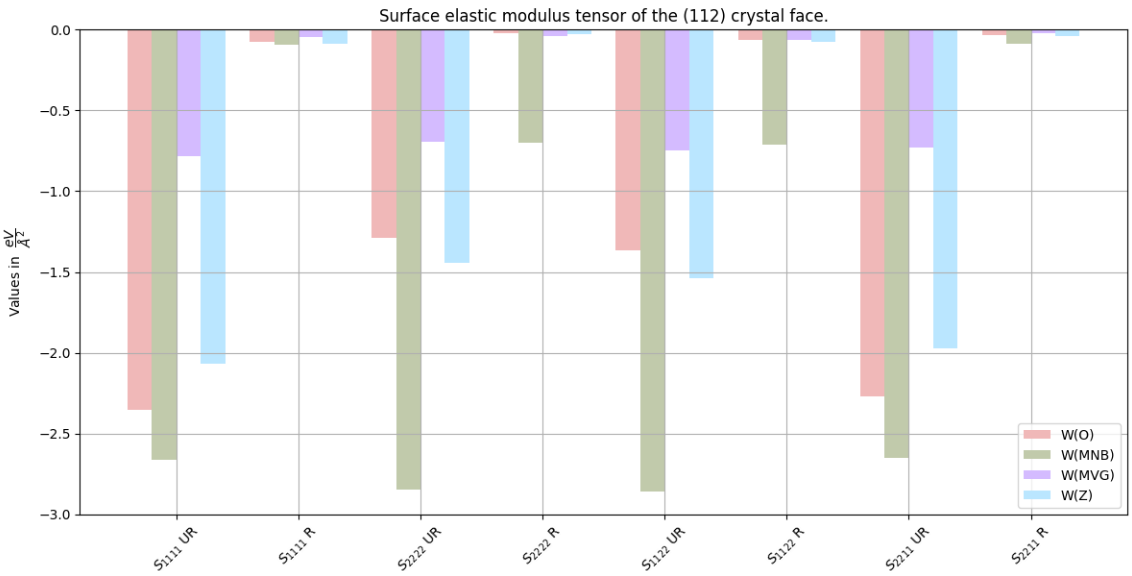

Figure 10: Graphic representation of the surface elastic modulus tensor of the (112) crystal face.

For most crystalline surfaces the previous studies support the idea of mainly negative surface elastic constants, which matches well with the calculated values. [36] It is evident that the values obtained after relaxing the surface are smaller in absolute values then those calculated during the stretching process. That is because after relaxing the surfaces are in a more stable state, which results in a smaller surface stress.

On average the values calculated for the surface elastic tensor of tungsten were 3-5 times bigger than the ones calculated for aluminium. The same is true for the Young moduli of these metals. With tungsten's Young modulus being around 400 GPa and aluminium's Young modulus is around 70 GPa [37 – 38].

Summary

The aim of this thesis was to calculate the surface elastic modulus tensor of tungsten using molecular dynamics method. In the current work, simulations of tungsten surfaces and bulk material were built to study the surface energy and surface stress without strain. Strain was applied on the systems to obtain polynomials that describe the surface energy of the systems depending on how much the initially created slab of material was strained. By applying strain in different directions and using the derivatives of the obtained polynomials, the surface elastic tensor for tungsten was obtained. Surface energy, surface stress at 0 strain and surface elastic moduli were calculated for 4 different cristallographic orientations using 4 different interatomic potentials and compared. It was found that the simulations using a potential developed by Marinica, Ventelon and Gilbert had the highest values for surface energy for every orientation studied as well as some of the largest values seen for surface elastic constants. Most of the surface elastic constants calculated stayed in a reasonable range.

5 References

1. H. Yanagisawa *et al.* Laser-induced asymmetric faceting and growth of nano-protrusion on a tungsten tip. *APL Photonics* **1,** 091305 (Nov. 2016).
2. V. Zadin. *Material surface modifications due to combined influence of femtosecond laser irradiation and applied electric fields* in (2019).
3. J. Meller. in *eLS* (John Wiley Sons, Ltd, 2001). ISBN: 9780470015902. eprint: `https://onlinelibrary.wiley.com/doi/pdf/10.1038/npg.els.0003048`. `https://onlinelibrary.wiley.com/doi/abs/10.1038/npg.els.0003048`.
4. M. S. Daw, S. M. Foiles & M. I. Baskes. The embedded-atom method: a review of theory and applications. *Materials Science Reports* **9,** 251–310. ISSN: 0920-2307. `https://www.sciencedirect.com/science/article/pii/092023079390001U` (1993).
5. M. S. Daw & M. I. Baskes. Embedded-atom method: Derivation and application to impurities, surfaces, and other defects in metals. *Phys. Rev. B* **29,** 6443–6453. `https://link.aps.org/doi/10.1103/PhysRevB.29.6443` (12 1984).
6. E. B. Tadmor & R. E. Miller. *Modeling Materials: Continuum, Atomistic and Multiscale Techniques* (Cambridge University Press, 2011).
7. D. C. Rapaport. in *The Art of Molecular Dynamics Simulation* ix–xi (Cambridge University Press, Cambridge, Apr. 2004).
8. P. H. Hünenberger. in *Advanced Computer Simulation* 105–149 (Springer Berlin Heidelberg, Jan. 2005). `https://doi.org/10.1007/b99427`.
9. Q. Ke, X. Gong, S. Liao, C. Duan & L. Li. Effects of thermostats/barostats on physical properties of liquids by molecular dynamics simulations. *Journal of Molecular Liquids* **365,** 120116. ISSN: 0167-7322. `http://dx.doi.org/10.1016/j.molliq.2022.120116` (Nov. 2022).
10. W. G. Hoover. Canonical dynamics: Equilibrium phase-space distributions. *Physical Review A* **31,** 1695–1697. `https://doi.org/10.1103/physreva.31.1695` (Mar. 1985).

11. D. J. Evans & B. L. Holian. The Nose–Hoover thermostat. *The Journal of Chemical Physics* **83,** 4069–4074. https://doi.org/10.1063/1.449071 (Oct. 1985).

12. V. B. Shenoy. Size-dependent rigidities of nanosized torsional elements. *International Journal of Solids and Structures* **39,** 4039–4052. ISSN: 0020-7683. https://www.sciencedirect.com/science/article/pii/S0020768302002615 (2002).

13. W Haiss. Surface stress of clean and adsorbate-covered solids. *Reports on Progress in Physics* **64,** 591–648. https://doi.org/10.1088/0034-4885/64/5/201 (May 2001).

14. H. Wasserman & J. Vermaak. On the determination of a lattice contraction in very small silver particles. *Surface Science* **22,** 164–172. https://doi.org/10.1016/0039-6028(70)90031-2 (Aug. 1970).

15. D. M. Duffy & J. H. Harding. Simulation of Organic Monolayers as Templates for the Nucleation of Calcite Crystals. *Langmuir* **20,** 7630–7636. https://doi.org/10.1021/la049552b (July 2004).

16. M. Methfessel, D. Hennig & M. Scheffler. Calculated surface energies of the 4d transition metals: A study of bond-cutting models. *Applied Physics A Solids and Surfaces* **55,** 442–448. https://doi.org/10.1007/bf00348331 (Nov. 1992).

17. R Shuttleworth. The Surface Tension of Solids. *Proceedings of the Physical Society. Section A* **63,** 444. https://dx.doi.org/10.1088/0370-1298/63/5/302 (1950).

18. R. M. Hackett. in *Hyperelasticity Primer* 5–8 (Springer International Publishing, Cham, 2016). ISBN: 978-3-319-23273-7. https://doi.org/10.1007/978-3-319-23273-7_2.

19. V. B. Shenoy. Atomistic calculations of elastic properties of metallic fcc crystal surfaces. *Phys. Rev. B* **71,** 094104. https://link.aps.org/doi/10.1103/PhysRevB.71.094104 (9 2005).

20. S. Izumi, S. Hara, T. Kumagai & S. Sakai. A method for calculating surface stress and surface elastic constants by molecular dynamics: application to the surface of crystal and amorphous silicon. *Thin Solid Films* **467,** 253–260. `https://doi.org/10.1016/j.tsf.2004.03.034` (Nov. 2004).

21. D. Hull. *Introduction to Dislocations* 4th ed. (ed Bacon, D. J.) (Butterworth-Heinemann, Woburn, MA, May 2014).

22. X. Liu, X. Kezhong & H. Zhai. Pressure Dependence of Structural and Mechanical Properties of Single-Crystal Tungsten: A Molecular Dynamics Study. *Metals* **11,** 1898 (Nov. 2021).

23. N. Waeselmann. *Structural transformations in complex perovskite-type relaxor and relaxor-based ferroelectrics at high pressures and temperatures* PhD thesis (May 2012).

24. A. P. Thompson *et al.* LAMMPS - a flexible simulation tool for particle-based materials modeling at the atomic, meso, and continuum scales. *Comp. Phys. Comm.* **271,** 108171 (2022).

25. A. Stukowski. Visualization and analysis of atomistic simulation data with OVITO-the Open Visualization Tool. *MODELLING AND SIMULATION IN MATERIALS SCIENCE AND ENGINEERING* **18.** ISSN: 0965-0393 (2010).

26. E. B. Tadmor, R. S. Elliott, J. P. Sethna, R. E. Miller & C. A. Becker. The potential of atomistic simulations and the knowledgebase of interatomic models. *JOM* **63,** 17–17. `https://doi.org/10.1007/s11837-011-0102-6` (July 2011).

27. F Ercolessi & J. B Adams. Interatomic Potentials from First-Principles Calculations: The Force-Matching Method. *Europhysics Letters (EPL)* **26,** 583–588. `https://doi.org/10.1209%2F0295-5075%2F26%2F8%2F005` (1994).

28. P. A. Olsson. Semi-empirical atomistic study of point defect properties in BCC transition metals. *Computational Materials Science* **47,** 135–145. `https://doi.org/10.1016/j.commatsci.2009.06.025` (Nov. 2009).

29. D. R. Mason, D Nguyen-Manh & C. S. Becquart. An empirical potential for simulating vacancy clusters in tungsten. *Journal of Physics: Condensed Matter* **29,** 505501. https://doi.org/10.1088/1361-648x/aa9776 (Nov. 2017).

30. E. Tadmor. *Finnis-Sinclair potential (LAMMPS cubic hermite tabulation) for W developed by Marinica et al. (2013); Potential EAM4 v000* 2018. https://openkim.org/cite/MO_046576227003_000.

31. E. Tadmor. *EAM potential (LAMMPS cubic hermite tabulation) for W developed by Zhou, Johnson, and Wadley (2004); NIST retabulation v000* 2018. https://openkim.org/cite/MO_914556822329_000.

32. S. Tian, J. Li, J. Zhang, Z. Wulabieke & D. Lv. Effect of Zr and Sc on microstructure and properties of 7136 aluminum alloy. *Journal of Materials Research and Technology* **8,** 4130–4140. https://doi.org/10.1016/j.jmrt.2019.07.022 (Sept. 2019).

33. U. Hansen, P. Vogl & V. Fiorentini. Quasiharmonic versus exact surface free energies of Al: A systematic study employing a classical interatomic potential. *Physical Review B* **60,** 5055–5064. https://doi.org/10.1103/physrevb.60.5055 (Aug. 1999).

34. J. Wang & S.-Q. Wang. Surface energy and work function of fcc and bcc crystals: Density functional study. *Surface Science* **630,** 216–224. https://doi.org/10.1016/j.susc.2014.08.017 (Dec. 2014).

35. H. N. Pishkenari & S. Rezaei. Characterization of silicon surface elastic constants based on different interatomic potentials. *Thin Solid Films* **626,** 104–109. https://doi.org/10.1016/j.tsf.2017.02.008 (Mar. 2017).

36. F. Ojaghnezhad & H. M. Shodja. A combined first principles and analytical treatment for determination of the surface elastic constants: application to Si(001) ideal and reconstructed surfaces. *Philosophical Magazine Letters* **92,** 7–19. https://doi.org/10.1080/09500839.2011.618813 (Jan. 2012).

37. C. Feng & B. S. Kang. Young's Modulus Measurement Using a Simplified Transparent Indenter Measurement Technique. *Experimental Mechanics* **48,** 9–15. https://doi.org/10.1007/s11340-007-9074-4 (Aug. 2007).

38. H.-J. Lunk & H. Hartl. Discovery, properties and applications of tungsten and its inorganic compounds. *ChemTexts* **5.** https://doi.org/10.1007/s40828-019-0088-1 (July 2019).

Lihtlitsents lõputöö reprodutseerimiseks ja lõputöö üldsusele kättesaadavaks tegemiseks

Mina, Kristi Koitla,

1. annan Tartu Ülikoolile tasuta loa (lihtlitsentsi) enda loodud teose "Calculation of the surface elastic modulus tensor of tungsten using molecular dynamics method", mille juhendajad on Andreas Kyritsakis ja Veronika Zadin

   1.1 reprodutseerimiseks säilitamise ja üldsusele kättesaadavaks tegemise eesmärgil, sealhulgas digitaalarhiivi DSpace'i lisamise eesmärgil kuni autoriõiguse kehtivuse tähtaja lõppemiseni;

   1.2 üldsusele kättesaadavaks tegemiseks Tartu Ülikooli veebikeskkonna kaudu, sealhulgas digitaalarhiivi DSpace'i kaudu kuni autoriõiguse kehtivuse tähtaja lõppemiseni.

2. olen teadlik, et punktis 1 nimetatud õigused jäävad alles ka autorile.

3. kinnitan, et lihtlitsentsi andmisega ei rikuta teiste isikute intellektuaalomandi ega isikuandmete kaitse seadusest tulenevaid õigusi.

Tartu, **31.05.2024**